RSC Advances

PAPER

View Article Online
View Journal | View Issue

Cite this: *RSC Adv.*, 2014, **4**, 46791

Theoretical study on optical and thermoelectric properties of the direct band gap α/β-Ca_2CdAs_2 pnictide semiconductors

Wilayat Khan* and Jan Minar

Received 5th July 2014
Accepted 3rd September 2014

DOI: 10.1039/c4ra06700b

www.rsc.org/advances

This article reports the utilization of the density functional theory within the Perdew–Burke–Ernzerhof generalized gradient functional for the electronic structure, optical and thermoelectric properties of the α-Ca_2CdAs_2 and β-Ca_2CdAs_2 single crystals. The theoretical calculations show that both the compounds are direct band gap semiconductors with optical band gaps of 0.96 eV and 0.79 eV at the point for α- and β-phases, respectively, which demonstrate that these compounds are optically active. The total and projected density of states, electronic charge density and optical properties, such as complex dielectric function, energy loss function, absorption coefficient, reflectivity and refractive index of α/β-Ca_2CdAs_2, were studied using the abovementioned technique. The calculated results for the energy band structures are compared with experimental and other simulated data. Temperature-dependent thermoelectric properties, such as electrical and thermal conductivity, Seebeck coefficient, power factor and figure of merit, were calculated. Our results show that α- and β-Ca_2CdAs_2 compounds are suitable materials for non-linear optical properties and thermoelectric devices.

1. Introduction

The Zintl phase group materials are intermetallic compounds composed of metals with varying electro-negativities belonging to the alkali and alkaline-earth metals, as well as transition metals and semimetals.[1] It has been demonstrated that the Zintl, Klemm and Wade's principles have good applicability in organic chemistry, which encourages the analysis of compositions, geometries and electronic structures. The Zintl approach can predict bonding behavior and can proffer the understanding of the properties that describe the main group of solid-state materials.[2] Many basic studies of the Zintl phase materials have been performed but work is required for nonlinear optical (NLO) applications. From previous work,[3] it could be deduced that the Zintl phase is appropriate in the infrared region (IR), in accordance with the prominent chalcopyrite semiconductors (ABC_2). For instance, ABC_2 semiconductors of $ZnGeP_2$ and $AgGaS_2$ are commercially available even though their high-power applications are restricted due to low laser damage thresholds. The A_2CdSb_2 material (A = Ca, Yb with Sr, Ba, Eu as dopants) might be an effective alternative due to the small energy gap and its non-centrosymmetric structural arrangement. Wang *et al.* studied novel ternary (Ca_2CdP_2, Ca_2CdAs_2, Sr_2CdAs_2, Ba_2CdAs_2 and Eu_2CdAs_2) Zintl materials of the orthorhombic Yb_2CdSb_2 structure. From the above studied compounds, the Ca_2CdAs_2 compound possessed monoclinic symmetry having the space group *Cm*. Thermal analyses revealed two polymorphs of the monoclinic phase, referred to as β-Ca_2CdAs_2 for the higher temperature and orthorhombic phase (α-Ca_2CdAs_2) for the lower temperature. They also concluded that the material possessed semiconducting properties. However, the detailed theoretical calculations on the structural and electronic properties of these pnictides (pnictogens) have not been studied.[3]

In the present work, we report the theoretical studies of the emerging α-Ca_2CdAs_2 and β-Ca_2CdAs_2 pnictide single crystals. Herein, we mainly focus on the electronic structure and optical properties of these materials by density functional theory. In addition, the predictions of thermoelectric properties using the semi-classical Boltzmann theory[4,5] are presented. The abovementioned techniques successfully explained the usefulness of optical properties and transport coefficients of both compounds for optoelectronic applications such as LEDs and thermoelectric materials.

2. Computational method

In this article, we have used the full potential linearized augmented plane wave (FP-LAPW) technique to calculate electronic structure and optical properties using the WIEN2k computer package.[6] Local density approximation by Ceperley Alder (LDA-CA)[7] and generalized gradient approximation by Perdew–Burke–Ernzerhof (GGA-PBE)[8] are used for exchange and correlation effects. α-Ca_2CdAs_2 has orthorhombic and β-Ca_2CdAs_2 has monoclinic crystal symmetry. The α-Ca_2CdAs

New Technologies-Research Centre, University of West Bohemia, Univerzitni 8, 306 14 Pilsen, Czech Republic. E-mail: walayat76@gmail.com; Tel: +420 775 526 684

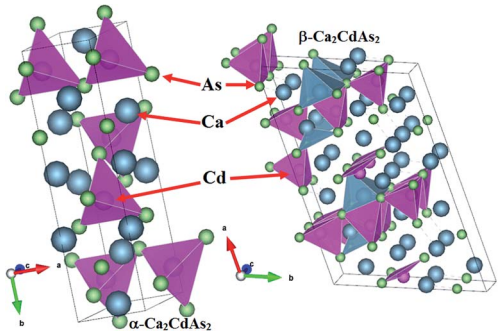

Fig. 1 Crystal structures of α/β-Ca_2CdAs_2.

and β-Ca_2CdAs_2 compounds have the space group symmetries of $Cmc2_1$ and Cm, respectively. The lattice parameters for α-Ca_2CdAs_2 are $a = 4.3163$ Å, $b = 16.5063$ Å and $c = 7.1418$ Å, while the lattice parameter for the β-Ca_2CdAs_2 are $a = 21.5152$ Å, $b = 4.3005$ Å and $c = 14.3761$ Å.[3] The crystal structure of the title compounds are shown in Fig. 1. The muffin tin sphere radii for Ca, Cd and As are 2.5, 2.5 and 2.36 atomic mass units for α-Ca_2CdAs_2 and 2.0, 2.0 and 2.0 atomic mass units for β-Ca_2CdAs_2, respectively. To control the size of the basis set for the wavefunction, we used the energy cut-off or plane wave cut-off ($R_{MT} \times K_{max}$) of 7.0. To calculate and converge the total energy, we used 344 k-points (α-Ca_2CdAs_2) and 405 k-points (β-Ca_2CdAs_2) in the irreducible Brillouin zone (IBZ). A dense mesh of 1500 k-points and 3000 k-points was used for the self-consistent calculation, which is very important for the optical properties of α/β-Ca_2CdAs_2.

The dielectric function $\varepsilon(\omega) = \varepsilon_1(\omega) + i\varepsilon_2(\omega)$ is known to indicate the optical response and is directly connected to the electronic structure. The imaginary part $\varepsilon_2(\omega)$ is computed from the momentum matrix elements between the probable transitions from high energy states in the valence band (VB) to the lower energy states in the conduction band (CB) over the Brillouin zone, and is given in ref. 9.

The real part $\varepsilon_1(\omega)$ is given by the Kramers–Kronig transformation. Other optical constants, such as reflectivity, absorption function and energy loss function, are derived from the calculated $\varepsilon_2(\omega)$ and $\varepsilon_1(\omega)$. We also calculated the electronic transport properties using the BolzTraP code at a constant relaxation time. The electronic transport coefficients are given in ref. 10.

After calculating, we can find other thermoelectric coefficients, such as the power factor and the figure of merit, of thermoelectric materials, which accurately explains the efficiency of the corresponding materials.

3. Results and discussions

3.1. Electronic structure

In order to obtain deeper insights into the electronic and optical properties of α/β-Ca_2CdAs_2 pnictide semiconductors, analyzing energy band structures is very helpful. We illustrated our calculated band structures along with the high symmetry lines of the Brillouin zone (BZ) in the k-space of the minimized structures within the LDA and GGA approaches for α/β-Ca_2CdAs_2, as shown in Fig. 2a–d. Both the functionals lead to very similar band dispersions. However, we obtained a considerable change in the band gap value. In particular, the value of the band gap predicted by the GGA-based calculation is in better agreement with the experimental value. In both α/β-Ca_2CdAs_2, the highest energy level bands and the lowest energy level bands are positioned at the Γ-point of the BZ, which exhibits direct band gaps. The calculated band gap values of 0.96 eV and 0.79 eV for the investigated compounds using the GGA approach are in close agreement to the experimental values and are better than the results from the previously simulated data.[5] The computed band gaps of α/β-Ca_2CdAs_2 are underestimated by about 4.0% and 21% compared to the experimental results of 1.0 eV.

We have plotted and compared the calculated total density of states of both compounds using LDA and GGA, as shown in Fig. 3a. In addition, in Fig. 3b–g we show element and angular momentum resolved densities of states for both the compounds. The lowest part of the valence band is mainly created from the Cd-d and As-s orbitals and small contributions are observed from the Ca/Cd-s/p orbitals of both compounds (Fig. 3). The upper part of the valence band is composed of the As-p orbital with a minor contribution from the Ca/As-s/p orbitals. As-p/d and Ca/Cd-s/p orbitals provide strong contributions to the conduction band of the partial density of states. One can clearly see that essential differences exist between the density of states of alpha (α) and beta (β) phases of Ca_2CdAs_2. The lower part at an energy −7.15 eV of α-Ca_2CdAs_2 possesses a prominent peak (27.0 states per eV) with a bandwidth of 0.76 eV and the lower part of β-Ca_2CdAs_2 at an energy of −8.63 eV indicates a maximum peak (25.2 states per eV) with a bandwidth of 0.78 eV. For both the compounds, As-p states are dominant over the entire valence band and show a prominent hybridization with Cd-s states at about −4.0 eV. In addition to the As-p states, bands at the top of the valence band have a Cd-p character, which corresponds to the Cd-s states found at the bottom of the conduction band. The upper part of the valence band of both the compounds has multiple peaks with a bandwidth of 3.1 eV.

3.2. Electronic charge density

We computed the electronic charge density (ECD) to understand the behavior of atoms in the compound by using the FP-LAPW method. To investigate the contact between Ca, Cd and As atoms in α/β-Ca_2CdAs_2, contour maps of electronic charge densities for GGA in the 2D (01–4 and 100) plane for α-Ca_2CdAs_2 compound was prepared, as demonstrated in Fig. 4a. We also plotted the electronic charge density for GGA in (010) and (001) planes for β-Ca_2CdAs_2, as shown in Fig. 4b to study the anisotropy in the electronic charge density by changing the planes. The ECD plot for both the compounds shows partial ionic and covalent bonding between As and Cd, as well as between As and Ca, which is explained by the Pauling electronegativity difference between As (2.18) and Ca/Cd (1.00/1.69) atoms. The calculated ECD shows that the charge density lines are spherical in some areas of the plane structure. This shows

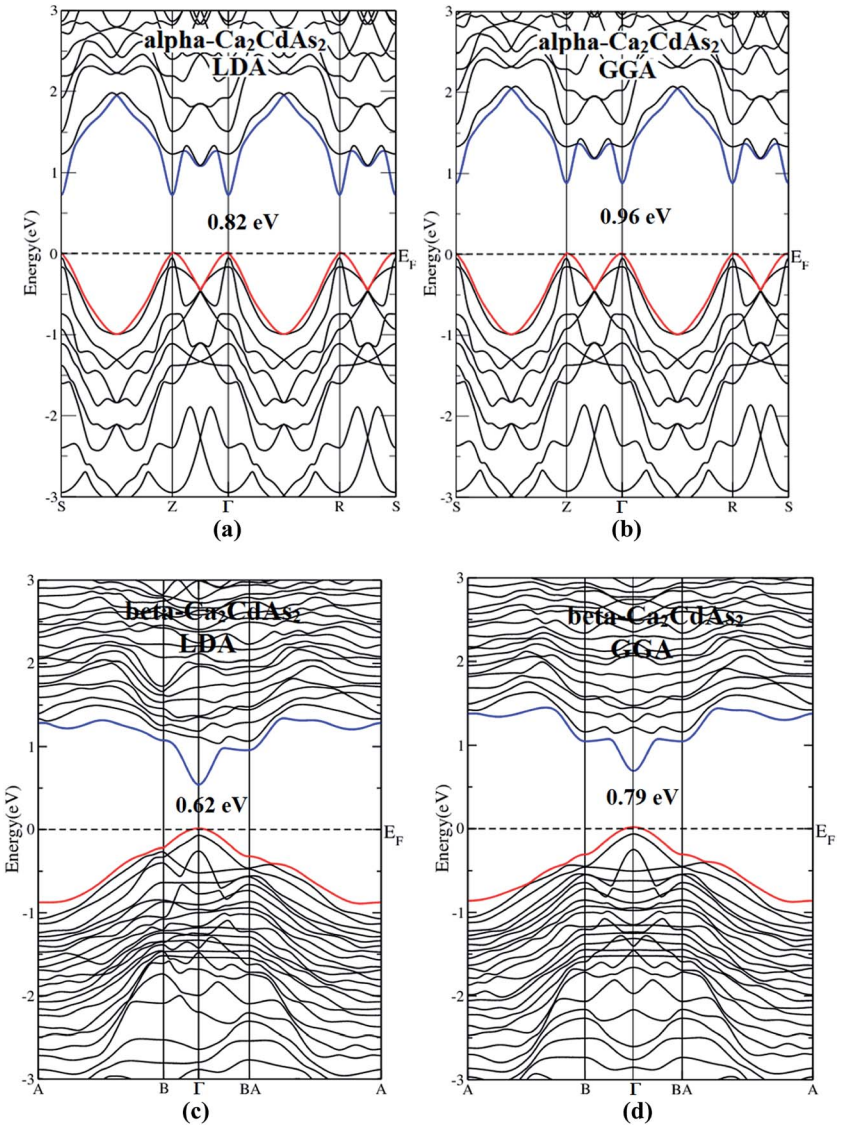

Fig. 2 Calculated (a and b) FP-LAPW band structures of α-Ca_2CdAs_2 and (c and d) FP-LAPW band structures of β-Ca_2CdAs_2, using LDA and GGA.

signs of ionic bonding between Ca and Cd atoms. In some areas, As and Cd/Ca atoms share electrons and show a strong covalent interaction between Ca–As and Cd–As. Because of the electronegativity differences between Cd and Ca atoms, most of the charges are transferred to the As site.

The electronic charge density (ECD) contour shows the anisotropy of the investigated compounds. It is clear from the ECD spectra of the α-Ca_2CdAs_2 compound that in the (01–4) plane the contribution of all the atoms has been shown, while in the (010) plane the Cd atom is absent. In the α-Ca_2CdAs_2 compound, the distance between As and Ca atoms in the (01–4) plane is smaller than the distance between the these two atoms in the (010) plane. In the β-Ca_2CdAs_2 compound the charge density around the As atom is weaker in the (100) plane, whereas in the (001) plane the charge density is greater around the As atom. In contrast to the (100) plane, in the (001) plane, bonding between As and Ca atoms was not observed.

3.3. Optical properties

As already mentioned in the introduction, Zintl phase materials are potential candidates with interesting non-linear optical properties. In the following section, we analyse in detail the optical properties for α/β-Ca_2CdAs_2 compounds. The spectra of the calculated imaginary part $\varepsilon_2(\omega)$ (in Fig. 5a) occurs only from direct band transitions and we have ignored the indirect band transitions that appear due to the scattering of phonons, which provide minor contribution to the dielectric function. The complex dielectric function can be successfully explained based on the calculated results of the electronic structure (band structure and density of states) and are closely related to each other.

The frequency dependent imaginary part $\varepsilon_2(\omega)$ of α/β-Ca_2CdAs_2 is shown in Fig. 5a. The computed $\varepsilon_2(\omega)$ has three main spectral peaks according to the symmetry, labelled by $\varepsilon_2^{xx}(\omega)$, $\varepsilon_2^{yy}(\omega)$, and $\varepsilon_2^{zz}(\omega)$ respectively, as shown in Fig. 5a. It should be noted that

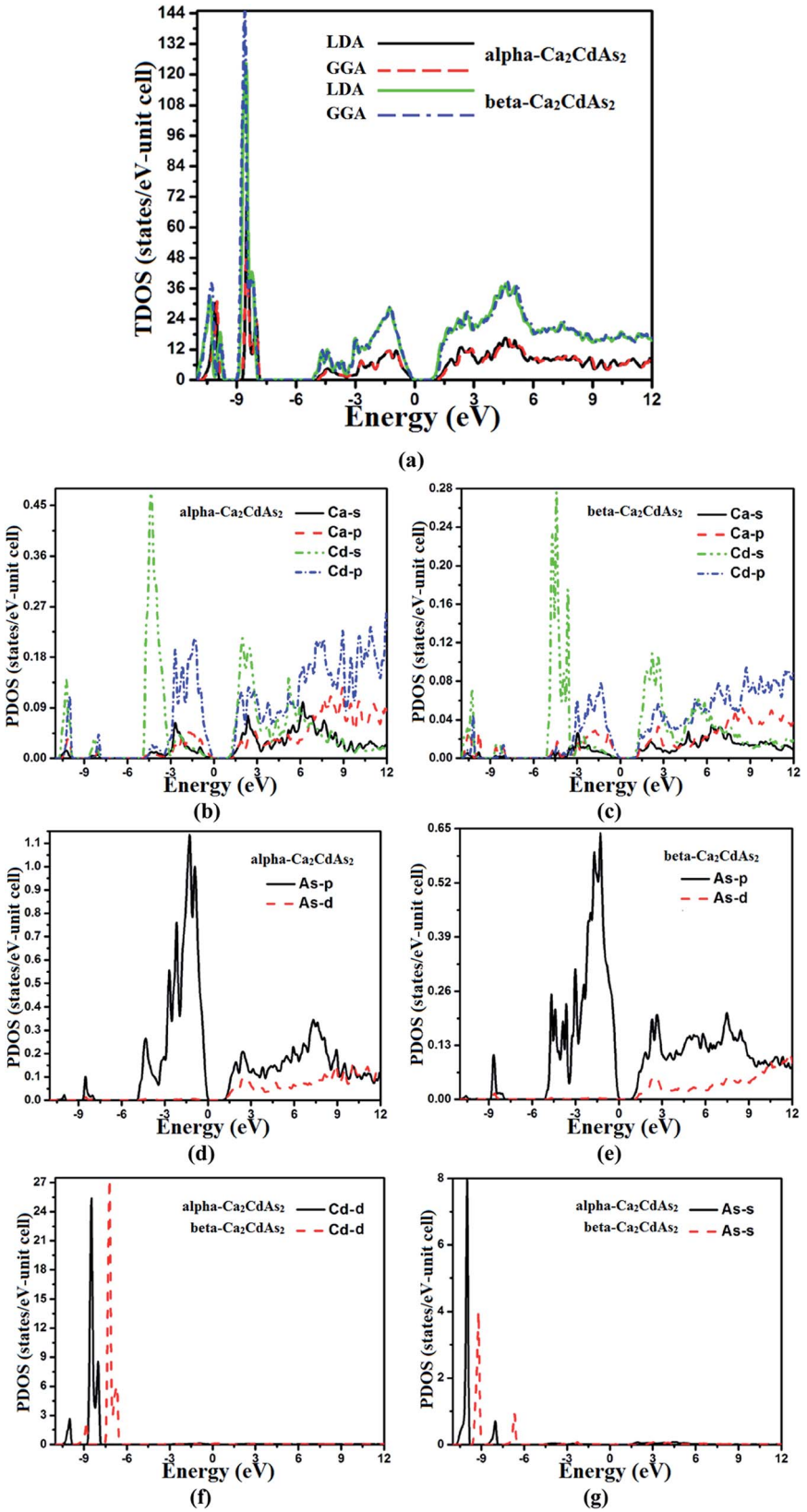

Fig. 3 Calculated FP-LAPW (a) total density state (TDOS) of α/β-Ca_2CdAs_2 using LDA and GGA and (b–f) partial density of states (PDOS) of Ca (s, p), Cd (s, p, d) and As (s, p, d), using GGA.

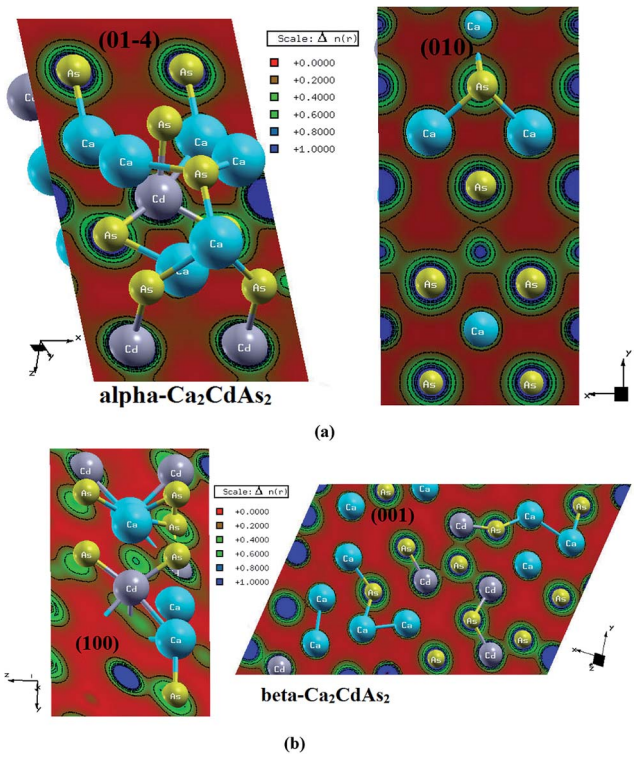

Fig. 4 Calculated electronic charge density along the crystallographic planes (a) the (01–4) and (010) planes of α-Ca_2CdAs_2 and (b) the (001) and (001) planes of β-Ca_2CdAs_2.

$\varepsilon_2(\omega)$ denotes the absorption spectra of the compounds and $\varepsilon_1(\omega)$ shows the refractive index at zero vibrations.

According to energy band structure calculations, the value of $\varepsilon_2(\omega)$ begins to increase at photon energies equal or greater than the band gap values of 0.96 eV and 0.79 eV in the case of α/β-Ca_2CdAs_2. For α/β-Ca_2CdAs_2, sharp peaks appeared at energies of about 4.0 eV and 26.0 eV. The transitions from As-p states of the high energy VB to the Cd-s states of the lower energy CB result in peaks at 4.0 eV, and the transitions from Cd-s (VB) to As-d (CB) states are responsible for the peaks at an energy of 26.0 eV in both the compounds. The calculated $\varepsilon_2(\omega)$ for both the compounds shows that the difference between the α- and β-phases is due to the decrease in the band gap. Fig. 5a indicates that there is an anisotropy in the mentioned energy range because the polarization along the *x*-axis is greater than that along the *y*/*z*-axes of α-Ca_2CdAs_2 and the polarization along the *x*/*z*-axes is greater than for the *y*-axis of β-Ca_2CdAs_2. It is very important to note that the peaks depending on $\varepsilon_2(\omega)$ are observed because of the many possible direct transitions, which might occur in the band structures. From the curve of the real part $\varepsilon_1(\omega)$ of the dielectric function, the static spectral components $\varepsilon_1^{xx}(\omega)$, $\varepsilon_1^{yy}(\omega)$ and $\varepsilon_1^{zz}(\omega)$ are 11.4, 12.5 and 11.2 for α-Ca_2CdAs_2 and 12.5, 12.6 and 11.8 for β-Ca_2CdAs_2, respectively (Fig. 5b). $\varepsilon_1(\omega)$ and the polarizability of the crystal are correlated, where the polarizibality is the distortion in the distribution of electrons in the corresponding states. Such distortions may be linked to the structure of the electron charge density.

The energy loss of fast moving electrons within a material is known as the energy loss function $L(\omega)$, which is shown in Fig. 5c. The peaks appeared in the curve of $L(\omega)$ for both the compounds due to plasma frequency resonance. The loss spectra for β-Ca_2CdAs_2 is more prominent in the far-ultra violet region (30.0 eV), while in the case of α-Ca_2CdAs_2 it appears in the mid-ultraviolet region (13.8 eV), as indicated in Fig. 5c. Peaks of the energy loss function $L(\omega)$ can be connected to the abrupt decrease in reflectivity $R(\omega)$.

Fig. 5d depicts calculated energy-dependent absorption spectra of both the compounds within the energy range from 0.0 to 35.0 eV. It is clear from Fig. 5d that when frequency ω exceeds the size of the band gap, the absorption coefficient $I(\omega)$ increases. This leads to a broad spectrum in the energy range from 4.0 to 10.0 eV. The three different polarization axes show sharp and maximum peaks at about 26.50 eV for $I^{xx}(\omega)$ and about 27.5 eV for both $I^{yy}(\omega)$ and $I^{zz}(\omega)$. It should be noted that both the investigated compounds possess higher absorption in the visible and near/far-ultraviolet region, which indicates that these materials are not transparent. The polarization components along *y*- and *z*-axes are nearly isotropic, while both show considerable anisotropy located between 5.0 to 9.5 eV and from 24.0 to 27.5 eV with the polarization component along the *x*-axis.

To gain more insight into these compounds, we calculated reflectivity coefficients $R(\omega)$, as shown in Fig. 5e. Both compounds show maximum reflectivity (52.0%) between the visible region and the near ultraviolet region, which decreases with energy and reaches a minimum value at 22.5 eV (Fig. 5e). The $R(\omega)$ spectra also have peaks (22.0%) at 27.8 eV. All the components of $R(\omega)$ show anisotropy from 5.0 eV to 11.0 eV, which is more pronounced in β-Ca_2CdAs_2 as compared to α-Ca_2CdAs_2. The energy range in which these compounds depict maximum reflectivity illustrates that they can transmit less radiation in the region and can be used as shielding materials.

The calculated refractive indexes $n(\omega)$ for both the compounds are illustrated in Fig. 5f. The static values of $n^{xx}(\omega)$, $n^{yy}(\omega)$ and $n^{zz}(\omega)$ are found to be 3.37, 3.54 and 3.36 for α-Ca_2CdAs_2 and 3.5, 3.6 and 3.4 for β-Ca_2CdAs_2, respectively (Fig. 5f). The value of $n(\omega)$ increases with energy in the visible region showing high transparency, decreases with energy in the ultraviolet region up to 15.0 eV and again increases up to 26.0 eV. It then reduces to lower values at 27.51 eV.

3.4. Thermoelectric properties

In this last section, we show our predicted thermoelectric properties to demonstrate the thermal stability of these materials and their possible thermoelectric applications. The temperature-dependent electronic thermoelectric properties of α/β-Ca_2CdAs_2 compounds are computed using the BoltzTraP code,[10] in terms of the calculated electronic structure, from 100 K to 800 K.

The electrical conductivity (σ) is expressed as:

$$\sigma = ne\mu \quad (1)$$

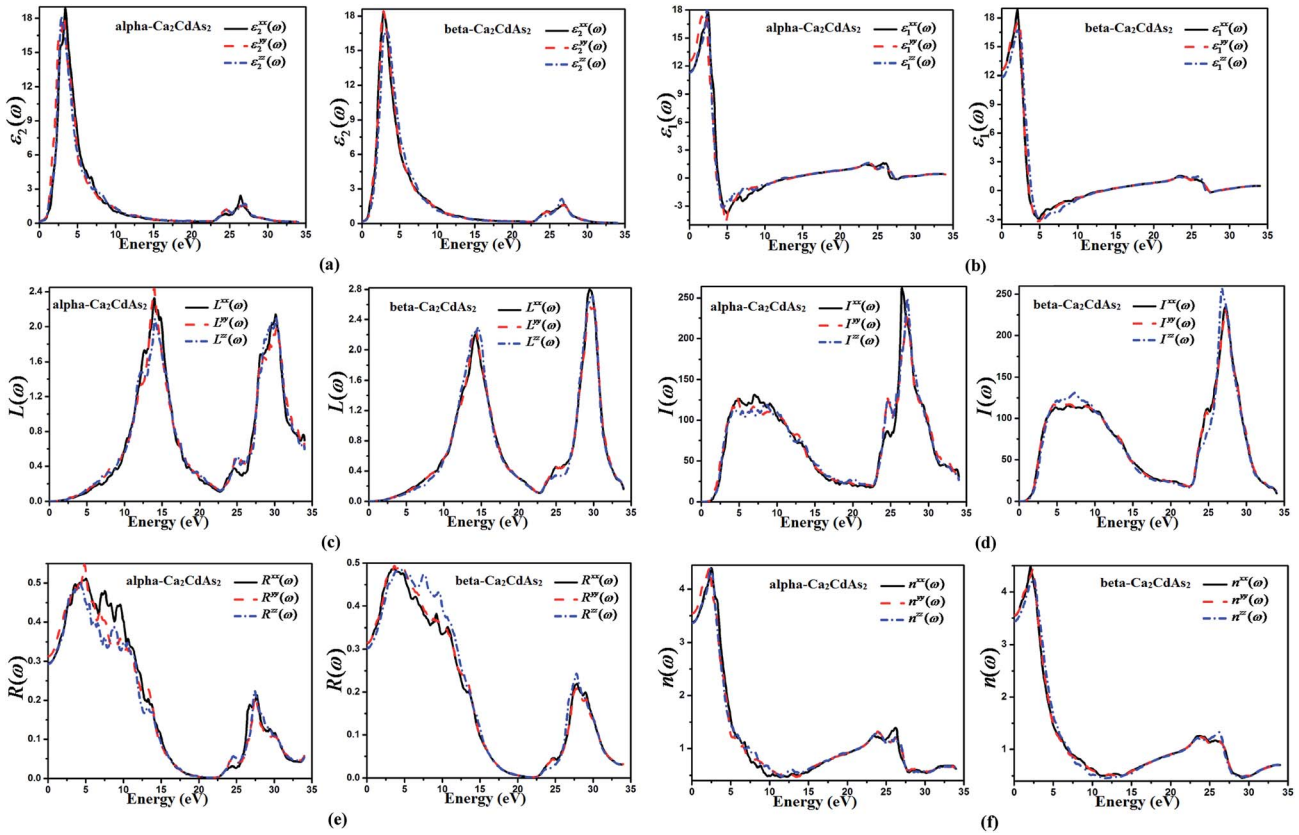

Fig. 5 Calculated (a and b) real and imaginary part of the frequency dependent dielectric function, (c) reflectivity, (d) energy loss function and (e) refractive index of α-Ca_2CdAs_2 (LHS) and β-Ca_2CdAs_2 (RHS), using GGA.

This equation shows that σ is influenced by both n and the mobility of the carrier, μ.

Fig. 6a shows the temperature-dependent electrical conductivity (σ^{ave}) over the relaxation time. The electrical conductivity of both the compounds exhibits anisotropy throughout the temperature range and exhibits an exponential growth on the increasing temperature from 50 to 800 K, which demonstrates that σ^{ave} obeys thermally generated behavior. At low temperatures (50 K), α-Ca_2CdAs_2 indicates a smaller value $(1.5(\Omega m\ s)^{-1})$ as compared to β-Ca_2CdAs_2 $(3.0(\Omega m\ s)^{-1})$, while at high temperatures (800 K), α-Ca_2CdAs_2 exhibits a greater value $(2.9(\Omega m\ s)^{-1})$ than β-Ca_2CdAs_2 $(2.25(\Omega m\ s)^{-1})$. Because the investigated compounds are semiconductors, both the carriers, *i.e.*, free and thermally generated charge carrier, contribute to electrical conductivity. The increase or decrease in σ^{ave} of α/β-Ca_2CdAs_2 also depends on the mobility of the carrier concentration because the mobility of the carriers is greater in α-Ca_2CdAs_2 than in β-Ca_2CdAs_2 (Fig. 6a). The reason for the decrease in the σ^{ave} of β-Ca_2CdAs_2 is the increase in carriers leading to pronounced scattering. This effect is due to the oscillation of carriers, which results in the reduction of mobility.[11]

Thermal conductivity (κ) in thermoelectric materials appears mainly from two sources: electrons and holes, which carry heat (κ_e) and phonons traversing through the lattice site (κ_l). The electronic thermal conductivity shows a direct relationship with electrical conductivity, as explained by the Wiedemann–Franz law:

$$\kappa = \kappa_e + \kappa_l \quad (2)$$

and

$$\kappa_e = L\sigma T = ne\mu LT \quad (3)$$

where L represents the Lorenz factor and its value is 2.4×10^{-8} $J^2\ K^{-2}\ C^{-2}$ for free carriers (electrons). The value of L changes due to the variation in carrier concentration. In small carrier (holes/electrons) concentration materials, an uncertainty arises in the electronic thermal conductivity due to two factors: when the Lorenz factor reduces by 20% from the number of free electrons and when the bipolar thermal conduction participates in the conduction process.[12]

We only analyze the electronic thermal conductivity because it plays an important role in the traveling electron limit. In fact, the Wiedemann–Franz law provides the transport mechanism according to which electrical/thermal currents are obtained from the mobility of the carrier concentration (at a low temperature). In general, this law is valid for elastic scattering mechanisms mainly used for determining electronic transport coefficients, which are applicable for normal energy band structures, suggesting that the variation in the energy caused by collision is smaller than K_BT.[13]

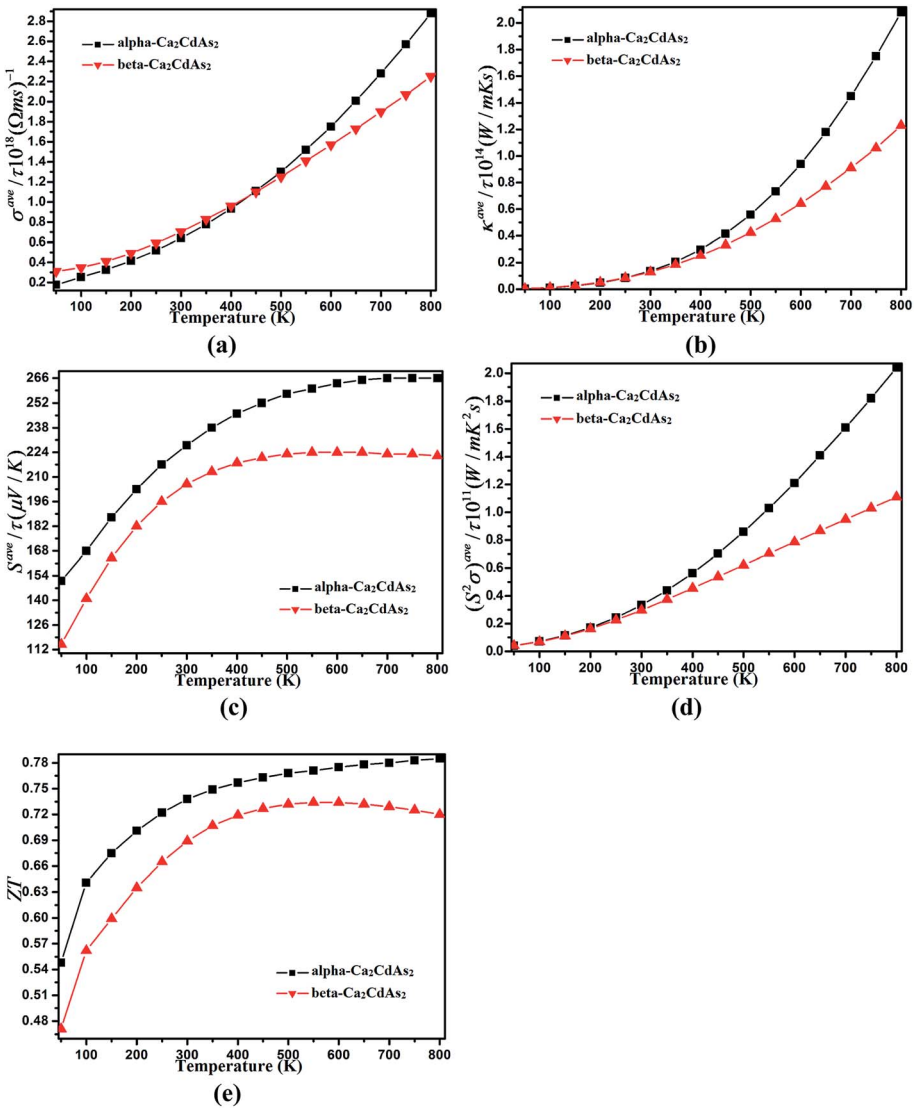

Fig. 6 Calculated transport coefficients of α-Ca_2CdAs_2 (LHS) and β-Ca_2CdAs_2 (RHS), using GGA as a function of Temperature (100–800 K): (a) electrical conductivity, (b) thermal conductivity, (c) Seeback coefficient, (d) power factor and (e) figure of merit.

The calculated average values of κ^{ave} of the investigated compounds are depicted in Fig. 6b as a function of temperature. It is obvious from Fig. 6b that κ^{ave} is small over the entire temperature range, which is normally expected for semiconducting compounds such as in our case of α/β-Ca_2CdAs_2. For both the compounds, κ^{ave} increases with temperature because of the increase in the mobility of electrons and narrow bands, but the behavior of both the compounds is quite different when the temperature goes beyond 400 K because κ^{ave}(α-Ca_2CdAs_2) increases sharply, while κ^{ave} (β-Ca_2CdAs_2) increases steadily with temperature. In both the compounds, minimum thermal conductivity is due to the random walk of electrons through the lattice. We should emphasize that α/β-Ca_2CdAs_2 remains stable along this temperature range. The calculated κ^{ave} can be analyzed in terms of three prominent parameters: temperature (T), carrier concentration (n) and mobility (μ). The value of κ^{ave} increases with the increase in temperature because the investigated compounds are semiconductors. By linearly increasing the number of charge carriers, κ^{ave} also increases due to the higher mobility of charge carriers. These effects are a consequence of the enhanced excitations of the carriers from VB to CB states due to increased temperature. Finally, from our results of σ^{ave} and κ^{ave}, which are based on the electronic structure, one can easily observe from the Fig. 6a and b that α/β-Ca_2CdAs_2 are very good thermoelectric materials and could be used as potential candidates for thermoelectric applications.

It is well-known that the Seebeck coefficient (S) presents a greater value for materials in which only one kind of carrier concentration (electrons/holes) contributes to thermal conduction. On the other hand, the Seebeck coefficient decreases if conduction is dominated by a high concentration of mixed carriers.

The Seebeck coefficient has an inverse relation with the carrier concentration (n), which is explained by the following mathematical relation:

$$S = \frac{8\pi^2 {k_B}^2}{3eh^2} m \times T\left(\frac{\pi}{3n}\right)^{2/3} \quad (4)$$

where m^* represents the effective mass of carriers.

The Seebeck coefficient of α-Ca_2CdAs_2 and β-Ca_2CdAs_2 is plotted as a function of temperature from 50 to 800 K under constant relaxation time, and is shown in Fig. 6c. In the comparison of the two compounds, one can find that the computed S^{ave} of α-Ca_2CdAs_2 is greater than that of β-Ca_2CdAs_2. It is clear from Fig. 6c that the magnitude of the Seebeck coefficient strongly depends on temperature because it increases with the increase in temperature and its maximum value 260 μV K^{-1} is obtained at 800 K. The positive Seebeck coefficient shows that both the compounds are p-type (hole) semiconductors (Fig. 6c). It is obvious from Fig. 6c that S^{ave} of α-Ca_2CdAs_2 increases on increasing the temperature from 50 to 800 K as compared to β-Ca_2CdAs_2 because the latter compound shows a maximum value of 240 μV/K at 550 K, which gradually decreases beyond 550 K. From eqn (4), it is also clear that the greater the carrier concentration the smaller S^{ave} will be, but the carrier concentration of α-Ca_2CdAs_2 is lower than that of the β-Ca_2CdAs_2. Therefore, S^{ave}/τ of the first compound still increases with temperature, as seen in Fig. 6c.

To obtain accurate information regarding the thermoelectric performance of both the compounds, we calculated the power factor and the figure of merit, which are plotted as a function of temperature, as presented in Fig. 6d and e. It is clear that the power factor only depends on the Seebeck coefficient and electrical conductivity, *i.e.*, P.F = $S^2\sigma$.

Larger power factors imply more efficient thermoelectric materials. $(S^2\sigma)^{ave}$ of both the compounds have the tendency to increase on increasing the temperature from 100 to 800 K. The variations in carrier concentrations and the accessible energy states in α/β-Ca_2CdAs_2 cause dispersion in the spectra, as depicted in Fig. 6d. The optimum values of $(S^2\sigma)^{ave}$ for α/β-Ca_2CdAs_2 are 2.05 × 10^{11} W mK^{-2} s^{-1} and 1.1 × 10^{11} mK^{-2} s^{-1}, respectively. Carrier concentration increases with increasing temperature, which then reduces the Seebeck coefficient (inverse relation with carrier concentration) and finally affects the $(S^2\sigma)^{ave}$. By summarizing all the results, we conclude that due to the high conductivity and high power factor of α-Ca2CdAs2 in comparison to the β phase, α phase is predicted to be a better choice for thermoelectric devices.

To finalize our study we calculated the figure of merit (ZT), which is given by:

$$ZT = \frac{S^2\sigma}{\kappa} T \quad (5)$$

The materials with high figure of merit need to have high electrical conductivity and low thermal conductivity. In our calculation, we cannot consider the lattice thermal conductivity caused by phonon scattering. The maximum values of $(ZT)^{ave}$ occur only when the electron and lattice thermal conductivity are comparable to each other. The calculated figure of merit $\left(ZT = \frac{S^2\sigma}{\kappa} T\right)$ for both α/β-Ca_2CdAs_2 reaches the values of 0.79 and 0.73 at temperatures 800 K and 500 K, respectively. The ZT value of α-Ca_2CdAs_2 is higher than that of β-Ca_2CdAs_2 because of the combination of light and heavy bands, *i.e.*, dispersive bands, which can increase the Seebeck coefficient. Our calculated results prove that both the compounds can be used for specific thermoelectric applications, especially for power generation.

4. Conclusions

Single crystals of pnictide semiconductors α/β-Ca_2CdAs_2 have been investigated by using the full potential linearized augmented plane wave method within the generalized gradient approximation. Our calculated electronic band structure depicts a direct optical band gap of 0.96 eV and 0.79 eV at the Γ-point, which is in close agreement with experimental and other computational data. From the calculated results of the total density of states and the partial density of states, we can conclude that the α-Ca_2CdAs_2 has a lower density of states than β-Ca_2CdAs_2 and we can also confirm that the As-p state possesses a maximum contribution to the highest valence energy band. The calculated ECD shows that there are covalent bonds between As and Cd/Ca atoms and ionic bonds between Ca and Cd atoms. We calculated the complex dielectric function, in which the maximum peaks are due to the interband transitions from the occupied to unoccupied bands and other optical parameters such as absorption, energy loss function, reflectivity and refractive index. Our calculations also suggest that these compounds are appropriate for optoelectronic applications in producing devices such as LEDs, and non-linear optical tools. Electronic transport properties are calculated using the BoltzTraP code under a constant relaxation time. The calculated results of the power factor and the figure of merit (0.79 and 0.73) suggest that both the compounds can be used for specific thermoelectric applications, especially for power generation.

Acknowledgements

This work was developed within the CENTEM project, reg. no. CZ.1.05/2.1.00/03.0088, co-funded by the ERDF as part of the Ministry of Education, Youth and Sports OP RDI program. MetaCentrum and the CERIT-SC under the program Centre CERIT Scientific Cloud, reg. no. CZ.1.05/3.2.00/08.0144. In addition we would like to acknowledge the EU-COST action MP1306 (EUspec).

References

1 S. Q. Xia and S. Bobev, *J. Am. Chem. Soc.*, 2007, **129**, 4049–4057.
2 M. T. Klem, J. T. Vaughey, J. G. Harp and J. D. Corbett, *Inorg. Chem.*, 2001, **40**, 7020–7026.

3 J. Wang, M. Yang, M.-Y. Pan, S.-Q. Xia and X.-T. Tao, *Inorg. Chem.*, 2011, **50**, 8020–8027.
4 J. M. Ziman, *Principles of the Theory of Solids*, Cambridge University Press, Cambridge, U.K, 1964.
5 G. K. H. Madsen and D. J. Singh, *Comput. Phys. Commun.*, 2006, **175**, 67.
6 P. Balaha, K. Shewartz, G. K. H. Madsen, D. Kvsnicka and J. Luitz, *WIEN2K, an Augmented Plane Wave +local Orbitals Program for Calculating Crystals Properties*, ISBN 3-9501031-1-2, Karlheinz Schewartz, Techn. Universitat, Wien Austria, 2001.
7 J. P. Perdew and Y. Wang, *Phys. Rev. B: Condens. Matter Mater. Phys.*, 1992, **45**, 13244.
8 J. P. Perdew, J. A. Chevary, S. H. Vosko, K. A. Jackson, M. R. Pederson, D. J. Singh and C. Fiolhais, *Phys. Rev. B: Condens. Matter Mater. Phys.*, 1992, **46**, 6671.
9 A. H. Reshak and W. Khan, *J. Alloys Compd.*, 2014, **591**, 362–369.
10 P. Poopanya, *et al.*, *Proceeding – Science and Engineering*, 2013, pp. 570–575.
11 M. Fox, *Optical Properties of Solids*, Oxford University Press, New York, 2001.
12 G. K. H. Madsen and D. J. Singh, 8 Feb 2006, Cond-mat.mtrl-sci.
13 G. A. Slack, in *CRC handbook of thermo-electrics Chemical Rubber*, ed. D. M. Rowe, Boca Raton, FL, 1995.